A mechanics-based perspective on the function of human sphincters during functional luminal imaging probe manometry

Guy Elisha[1], Sourav Halder[2], Dustin A. Carlson[3], Wenjun Kou[3], Peter J. Kahrilas[3], John E. Pandolfino[3], and Neelesh A. Patankar*[1,2]

[1]Department of Mechanical Engineering, McCormick School of Engineering, Northwestern University, Evanston, IL 60201, USA

[2]Theoretical and Applied Mechanics Program, McCormick School of Engineering, Northwestern University, Evanston, IL 60201, USA

[3]Division of Gastroenterology and Hepatology, Feinberg School of Medicine, Northwestern University, Chicago, IL 60611, USA

Abstract

Functional luminal imaging probe (FLIP) is used to measure cross-sectional area (CSA) and pressure at sphincters. It consists of a catheter surrounded by a fluid filled cylindrical bag, closed on both ends. Plotting the pressure-CSA hysteresis of a sphincter during a contraction cycle, which is available through FLIP testing, offers information on its functionality, and can provide diagnostic insights. However, limited work has been done to explain the mechanics of these pressure-CSA loops. This work presents a consolidated picture of pressure-CSA loops of different sphincters. Clinical data reveal that although sphincters have a similar purpose (controlling the flow of liquids and solids by opening and closing), two different pressure-CSA loop patterns emerge: negative slope loop (NSL) and positive slope loop (PSL). We show that the loop type is the result of an interplay between (or lack thereof) two mechanical modes: (i) neurogenic mediated relaxation of the sphincter muscle or pulling applied by external forces, and (ii) muscle contraction proximal to the sphincter which causes mechanical distention. We conclude that sphincters which only function through mechanism (i) exhibition NSL whereas sphincters which open as a result of both (i) and (ii) display a PSL. This work provides a fundamental mechanical understanding of human sphincters. This can be used to identify normal and abnormal phenotypes for the different sphincters and help in creating physiomarkers based on work calculation.

Keywords: sphincter, esophagus, peristalsis, pressure-area hysteresis, functional luminal imaging probe, manometry

Nomenclature

A	Tube cross-sectional area
A_o	Undeformed reference cross-sectional area (or rest area)
K_e	Tube stiffness
L	Tube length
P	Pressure inside the tube

*Corresponding author: N. A. Patankar (n-patankar@northwestern.edu)

P_o	Pressure outside the tube
p	Non-dimensional pressure inside the tube
p_o	Non-dimensional pressure outside the tube
U	Non-dimensional fluid velocity (averaged at each cross-sectional area)
u	Fluid velocity (averaged at each cross-sectional area)
$S_{\mathbf{IC}}$	Constant cross-sectional area that depends on bag volume
t_R	Sphincter relaxation time
α	Non-dimensional tube cross-sectional area
β	Dimensionless strength of viscous effects (inverse of Reynolds number)
θ	Activation function
μ	Fluid viscosity
ρ	Fluid density
ψ	Dimensionless rigidity of the elastic tube (inverse of Cauchy number)

1 Introduction

A sphincter is a tonically contracted circular muscle which controls the flow of liquids and solids. For example, the lower esophageal sphincter (LES) monitors the entrance of swallowed matter from the esophagus into the stomach while preventing retrograde flow from the stomach into the esophagus (acid reflux) [1]. The human body includes many sphincters, with main examples listed in table 1. Dysfunction of sphincters is the root cause of many physiological disorders, especially along the GI track [2]. In the case of the LES, dysfunction can be either excessive compliance causing retrograde acid flow into the esophagus (such as in gastroesophageal reflux disease [3, 4]) or absence of LES relaxation preventing healthy opening of the sphincter and emptying of the esophagus (such as in achalasia [5, 6]). Hence, it is important to understand the mechanical function of the sphincters, and particularly, their opening and closing mechanisms [2].

As noted by [2], a functional luminal imaging probe (FLIP) has increasingly become one of the more useful tools to determine the shape of a sphincter. The FLIP consists of a catheter and a bag which is placed inside a channel (such as the anal canal), bypassing the sphincter. The FLIP measures cross-sectional area (CSA) and pressure in the bag as a function of time, as the walls of the sphincter respond to the filling of the bag [21, 22]. The FLIP bag length and volume depends on the experimental set up. For example, in the FLIP study on the anal sphincter (AS) by [23], the bag length was 30 mm, and the maximum bag volume was 90 ml. In a FLIP study by [24] on the esophagus, the FLIP bag length was 16 cm, and the maximum bag volume was 60 ml. Figure 1 presents an illustration of a FLIP device used in the esophagus.

The procedures themselves also differ based on the physiology of the sphincter. For instance, in the case of the esophagus and the LES, the contraction and relaxation during a FLIP testing is mainly involuntary. As the volume of the bag increases, it triggers distention induced peristalsis, which varies the CSA and bag pressure [24]. On the other hand, [23] study captured voluntary contraction of the AS (active squeezing of the sphincter muscle).

The FLIP has become increasingly popular since it allows distensibility testing; the sphincter's resistance to distention. This evaluation can be easily done using FLIP over other measuring devices. Hence, it is known to be the superior approach in evaluating the condition of a sphincter [2, 25].

Table 1: List of sphincters in the human body

Sphincter	**Description**
Upper esophageal sphincter (UES)	A C-shaped striated muscle sphincter attached to the lateral aspects of the cricoid cartilage [7]. It does not have a resting tone, but rather responds to a vast array of reflexive inputs [7]. Its main function is to monitor the flow coming into and out of the esophagus. During respiration, the UES is to remain occluded to prevent air from entering the esophagus and the esophagus content from flowing back into the mouth. During swallowing, the UES opens to allow bolus transport from the mouth into the esophagus [8, 9].
Lower esophageal sphincter (LES)	Tonically contracted composite of different muscles located at the distal end of the esophagus. The LES moderates the entrance of swallowed material coming from the mouth through the esophagus into the stomach while preventing gastroesophageal reflux [1, 10, 11].
Pyloric sphincter (PS)	Circular muscle layer connecting between the pylorus and the duodenum which controls the flow of stomach discharge into the duodenum [12, 13]. Its function and opening depends on the phase: digestive or inter-digestive.
Sphincter of Oddi (SoO)	Tonically contracted at rest, located at the end of the ampulla (between ampulla and small intestine). The SoO regulates the flow of bile and pancreatic juice into the small intestine and prevents reflux of small intestine content into the ampulla [12, 14].
Internal anal sphincter (IAS)	Smooth muscle sphincter located around the anal canal [12]. It is always in a state of tonic contraction which is maintained by sympathetic fibers to prevent leakage [12]. The sphincter relaxes involuntary when sufficient fecal material accumulates in the canal [12, 15]. This does not imply defecating since the EAS also plays a role [12].
External anal sphincter (EAS)	Striated muscle sphincter located around the IAS [12]. It is always in a state of tonic contraction to keep the anal canal shut and prevent leakage. Once a voluntary signal is sent to relax the sphincter, it opens and allows the passage of feces out of the body [12]. The EAS can be further contracted (occluded) voluntarily [12].
Internal urethral sphincter (IUS)	Smooth muscle fibers located at the junction of the urethra with the urinary bladder [16]. Its main role, together with the EUS, is to control the flow of urine [12]. The IUS is an involuntary sphincter that is tonically contracted at rest and relaxes during micturition [16, 17]. The relaxation is controlled by the nervous system [18]. For males, the IUS is also responsible for preventing retrograde flow of semen into the bladder during ejaculation [12, 19].
External urethral sphincter – female (EUSF)	Fibrous muscle which surrounds the urethra in the middle third of its length [16]. It is located between the vaginal orifice and the clitoris [19]. The EUSF is a voluntary sphincter which is tonically contracted to prevent the leakage of urine. Once it relaxes and opens, it allows the flow of urine out of the body [12, 20].
External urethral sphincter – male (EUSM)	Circular muscle fibers located between the pudendal canals and below the pelvic diaphragm [19]. The sphincter muscles are tonically contracted to prevent leakage of urine, and relax voluntary to allow voiding [12].

Borrowed from cardiovascular assessment, one approach taken to study the mechanical function of sphincters is by tracking its pressure and CSA during an opening and closing cycle [2]. Plotting the pressure-CSA hysteresis of a sphincter offers information on its functionality and can provide diagnostic insights. Moreover, it unveils the way in which work is done and expended during a contraction cycle [2, 26]. Producing a pressure area loop at the sphincter was made possible by FLIP testing.

Our goal is to provide a framework in which we can investigate the function of different sphincters. In this work, we seek to provide a mechanics-based perspective on the function of human sphincters during FLIP manometry. While many studies have used FLIP to evaluate sphincter functionality, to our knowledge, no work has been done to create a common understanding of FLIP data across different sphincters. In addition, limited work has been done to explain the mechanics of the pressure-CSA loops at the different sphincters. Thus, in this study, we aim to find pressure-CSA hysteresis characteristics for each sphincter and identify the mechanisms that create such patterns. We explain the sphincter opening and closing pattern by reproducing them using simulations and looking at the work done by the sphincter wall throughout an opening and closing cycle.

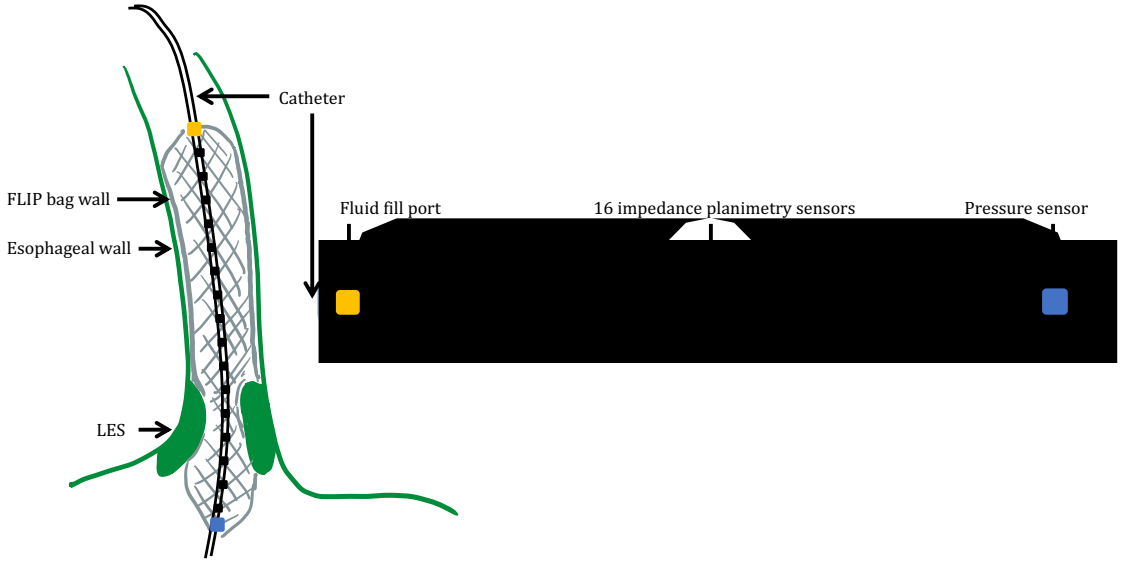

Figure 1: Diagram showing the FLIP bag and catheter assembly placed within the esophagus, bypassing the LES. In many esophageal FLIP studies, the FLIP's bag is 16 cm long and 22 mm in diameter. The catheter measures CSA at 16 location and one pressure measurement at each time instance.

2 Analysis of Literature Data

Table 2. presents a summary of studies which used FLIP or FLIP-like devices to investigate and report pressure and CSA values at different sphincters. Out of these studies, only two have plotted the pressure-CSA loops at the sphincter during a single contraction cycle, one for the anal sphincter (AS) and the other for the LES (see Fig. 2a and Fig. 2b.) The study by [27] on the Sphincter of Oddi (SoO) presents curves for pressure vs. CSA during a pressure ramp, as shown in Fig. 2c, but not a complete loop. To the best of our knowledge, no clinical pressure-CSA loops, during a single contraction cycle, have been plotted for the other sphincters listed in table 1.

Note that many studies have reported pressure-CSA loops at both female urethral sphincter (FUS), and male urethral sphincter (MUS) using a FLIP-like device of a catheter surrounded by a cylindrical shaped bag [28, 29, 30]. However, these loops do not represent a single contraction cycle. Each point on the loop depicts pressure and CSA at a different bag volume. We did not find any studies capturing pressure and CSA behavior of the urethral sphincter (US) with a bag of constant volume.

From Fig. 2, we can identify two different loop types:

(i) Negative slope loop (NSL). Pressure increases as CSA of the sphincter decreases, such as in Fig. 2a. A similar pattern is seen in Fig. 2c.

(ii) Positive slope loop (PSL). Pressure increases as CSA of the sphincter increases, such as in Fig. 2b.

If all sphincters relax and contract, why do we see different loop patterns (positive and negative slopes)? We aim to answer this question. We wish to investigate the different pressure-CSA loop patterns and reveal the underlying reason which leads to the different loops at different sphincters. We hypothesize that the loop types are a result of different muscle activities at the sphincter and the location upstream to the sphincter. In particular, we hypothesize that the loop type is dictated by the presence (or absence) of two mechanical modes discussed next.

Table 3. lists and describes the opening and closing mechanisms of each sphincter as obtained from literature survey. There are two potential mechanisms to open sphincters:

(i) Neurogenic mediated relaxation of the sphincter itself

Table 2: List of literature of FLIP and FLIP-like studies at the different sphincters

Reference	Placement	Bag geometry	Subjects (n)	Description
[31]	UES	25-mm diameter 10-cm long	11 (controls)	The FLIP bag was placed across the UES and the bag was filled. The CSA and pressure in the bag were measured during wet and dry swallows at each bag volume (5,10,15,20 mL).
[32]	LES	25-mm diameter 6.4-cm long	20 (controls) 20 (patients)	The FLIP device was inserted into the esophagus lumen, passing through the esophagus. The CSA at 16 locations and one distal pressure measurements were taken as a function of time at 10- to 40-mL volume.
[26]	LES	22-mm diameter 16-cm long	24 (controls)	Same as procedure above with a longer bag, and experiment conducted at 50- and 60-mL volume.
[33]	PS	25-mm diameter 12-cm long	21 (controls) 32 (patients)	The catheter was inserted trans-nasally, and the bag was positioned such that it passes through the pylorus. The bag volume was set to 10, 20, 30, and 40-mL. Pressure and CSA were reported at stable condition (not over time) so peristaltic effects on their values are not captured.
[34]	PS	EndoFLIP device	54 (patients)	The catheter was inserted orally, and the bag was positioned such that it passes through the pylorus. The bag volume was set to 20, 30, 40, and 50-cc. The recorded P and CSA were taken from a single time instance.
[27]	SoO	9-mm diameter 5-cm long	4 (patients)	The probe was inserted into the SoO and the bag was filled at a rate of 1-mL/min. During this process, the CSAs and pressures were recorded.
[23]	AS	30-mm diameter 90-mL maximal volume	14 (F - controls) 14 (F - patients)	FLIP bag was placed in the AS. Three, 10-sec maximum voluntary squeezes were performed at each bag volume (50,70,90-mL).
[35]	AS	25-mm diameter 12-cm long	40 (F - controls) 34 (F - patients)	FLIP was inserted in the rectum. The bag volume was set to 10, 20, 30, 40, or 50-mL and the participants were asked to squeeze the filled bag.
[28]	US-F	5-mm diameter 6-cm long	143 (subjects)	The catheter surrounded by an elastic, cylindrically shaped bag was placed inside the urethra, passing through the sphincter. The bag volume increased systematically by a controlled, stepwise, inflation and deflation of the bag with air. The P and CSA at each time increment was recorded. The experiment was conducted in both relaxed and squeezed state.
[29]	US-M	7.5-mm diameter 5-6-cm long	10 (subjects)	Similar experimental set up as described above.

(ii) Peristaltic contraction or some squeezing upstream of the sphincter that causes mechanical distention.

A sphincter's opening function can be defined by either only mechanism (i) (Case 1), or a combination of (i) and (ii) acting together (Case 2). Case 1 refers to sphincters which open only because of tonic relaxation of the sphincter muscle, like the AS [12, 36]. This neurally controlled muscle activity can be either voluntary or involuntary. Case 2 refers to sphincters which open as a result of the two mechanisms. While the sphincter muscles relax, there is also peristalsis of some sort proximal to the sphincter which increases the pressure, causing mechanical distention, like in the LES [26, 11]. Note that for the second mechanism to be considered, the pressure in the lumen must play a role in the sphincter's opening. The anal canal for instance is a high-pressure zone which increases as the canal is getting filled. However, this increase in pressure triggers the

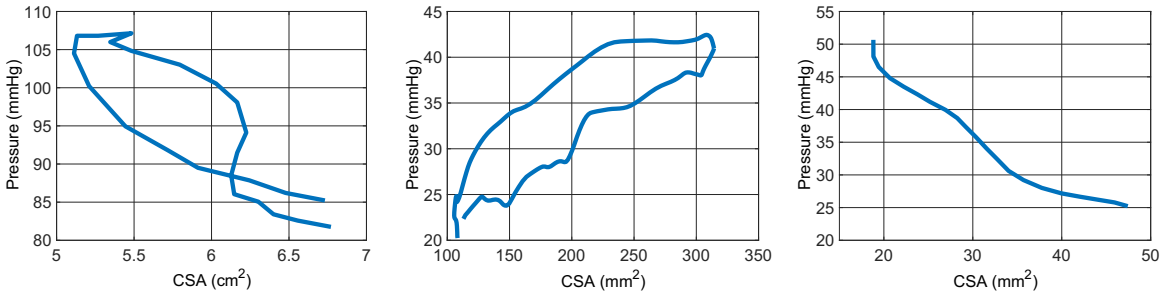

(a) AS by [23] (b) LES by [26] (c) SoO curve by [27]

Figure 2: Pressure-CSA plots obtained by FLIP experiments reported in literature.

internal sphincter to relax but is not mechanically involved in the opening process itself [15, 37].

Note that different from other sphincters, the upper esophageal sphincter (UES) does not have a resting tone, but rather responds to a vast array of reflexive inputs. It does not open due to muscle relaxation nor mechanical distention, but by anterior traction on the cricoid cartilage, which forces the sphincter to open [7]. The UES opening is a result of pulling applied by external forces. With that said, the mechanical imprint is equivalent to relaxation of the tone. Thus, we classify the UES's opening by mechanism (i) (Case 1). We will later show that whether the sphincter opens due to neurogenic mediated relaxation or due to neurally controlled pulling of the sphincter wall, the pressure-CSA loop type is not affected.

3 Methods

Given our understanding of the sphincters' functions from literature (table 3), we can reproduce their opening and closing mechanisms using simulations. Simulations allow us to dictate the activation function, imitating the muscle's activity throughout a contraction cycle. Doing so can help us in identifying which muscle activation configurations result in each loop type.

In our previous studies, we developed a 1D model of a fluid filled elastic tube which is closed on both ends in order to mimic a flow inside a FLIP device [38, 39, 26]. Our goal was to study the relation between the tube's wall properties, fluid properties, muscle activation pattern, and their effect on pressure inside the tube and the tube's resulting shape. In this work, we build on and extend the pervious model by introducing different forms of the muscle pattern to account for the functions of the different sphincters. In this section, we briefly introduce the mathematical configuration of the 1D model. Extended description is available in [38, 26].

3.1 Governing Equations in 1D

The 1D mass and momentum conservation equations were derived in [45] and take the form

$$\frac{\partial A}{\partial t} + \frac{\partial (Au)}{\partial x} = 0, \tag{1}$$

and

$$\frac{\partial u}{\partial t} + u\frac{\partial u}{\partial x} = -\frac{1}{\rho}\frac{\partial P}{\partial x} - \frac{8\pi\mu u}{\rho A}, \tag{2}$$

respectively [39]. Here, $A(x,t)$, $u(x,t)$, $P(x,t)$, ρ and μ are the tube CSA, fluid velocity (averaged at each cross-sectional area), pressure inside the tube, fluid density, and fluid viscosity, respectively. To complete

Table 3: Sphincters and their opening modes

Sphincter	**Process Description**	**Mechanism**
UES	During swallowing, the UES opens through anterior traction on the cricoid cartilage by the strap muscles suspending the hyoid bone [7, 8, 40]. Once the UES is open, the bolus is transferred through the UES into the esophagus by tongue pulsion followed by peristaltic contraction [8].	(i)
LES	After the bolus enters the esophagus through the UES, a peristaltic contraction pushes it towards the LES [1]. The peristaltic activity, together with active tone relaxation of the LES muscle open the LES and allow the emptying of the esophagus content into the stomach [26, 11].	(i) + (ii)
PS	During the digestive state, antral contractions push the food against the constricted pylorus which only allows the passage of small particles [41]. The remainder of the chyme is propelled backwards and is subject to additional antral contractions. Only during the inter-digestive period, the migrating motor complex is activated to clear indigestible material from the stomach [42] Intragastric pressure is developed by a peristaltic wave passing through the antrum, causing the pylorus to open sufficiently wide to allow that material to exit [43, 13].	(i)+(ii) (during inter-digestive)
SoO	There is no musculature in the bile duct or the pancreatic duct. Consequently, the pumping action is done by the sphincter itself. This can be triggered by the injection or secretion of cholecystokinin. Cholecystokinin triggers propagated contractions within the sphincter that milk bile or pancreatic secretions into the duodenum [14, 44]. Hence, the opening occurs by the sphincter itself relaxing with some help from pressurization.	(i)+(ii) (small effect from (ii)).
IAS	Once enough fecal material accumulates the rectum, it causes the rectum to distend, triggering the sphincter to tonically relax (nerval response) [12, 36, 15]. Peristalsis is not involved, and the opening does not depend on mechanical distention [15, 37].	(i)
EAS	When the IAS relaxes (involuntarily), it signals the need for the body to defecate [12]. The EAS remains contracted, even after the IAS opens, unless a voluntary signal to defecate is in place [12]. Once the signal to relax is received, the anorectal angle decreases, allowing the EAS to open [12]. Following the opening, peristaltic waves and rectum contraction forcing fecal material out of the anal canal [12]. This peristalsis does not play a mechanical role in the opening of the sphincter as it takes place after the sphincter has opened.	(i)
US	Since the internal and external sphincters are interdependent, we refer to their opening and closing function as one unit, the US. The sympathetic nervous system is responsible of keeping the US contracted, while the parasympathetic nervous system is responsible for relaxing the sphincter once the bladder is sufficiently full [16, 17]. The relaxation of the muscle causes the sphincter to open and allow flow into the urethra [12, 16, 17]. Thus, the opening is neurally controlled. Peristalsis contraction force urine towards the external urethral orifice. However, the peristaltic activity at the urethra occurs distal to the urethral sphincter and therefore is not mechanically involved in the opening process of the sphincter.	(i)

the system, we introduce a constitutive equation for pressure, which relates pressure and CSA, such that

$$P = K_e \left(\frac{A(x,t)}{A_o \theta(x,t)} - 1 \right) + P_o. \tag{3}$$

The equation above, also known as the 'tube law', was derived by [46] and validated experimentally by [47]. In the equation above, P_o is the outside pressure, K_e is tube stiffness, and A_o is the undeformed reference area (CSA of the tube when $\Delta P = P - P_o = 0$). The term $\theta(x,t)$ is called the activation function, implemented to the model in order to mimic muscle contraction and relaxation by changing the reference CSA of the tube wall [48, 49]. When $\theta = 1$, there is no contraction nor relaxation, and the system is fully at rest. When $\theta < 1$, contraction is implemented. The smaller the value of θ, the smaller the tube reference area, and the greater the contraction intensity. When $\theta > 1$, relaxation is implemented.

Recall that in the case of the UES, no muscle relaxation is present, but rather external traction which pulls the sphincter's wall to open. To simulate this scenario, we vary the value of P_o over time, such that

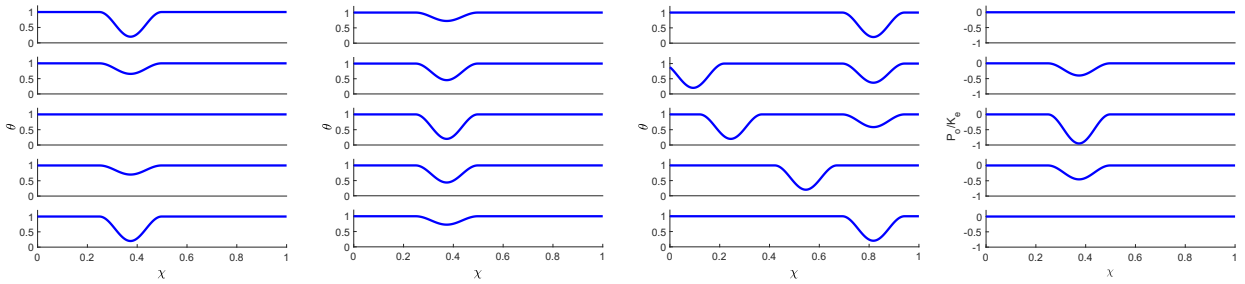

(a) Tone relaxation (b) Tone squeezing (c) Tone and peristalsis (d) Outside pressure

Figure 3: Illustrations of the four activation functions used for the simulations in this study. Each subfigure presents five consecutive instances. Figures (a),(b), and (c) present different $\theta(x,t)$ functions while figure (d) presents $P_o(x,t)/K_e$.

$P_o = P_o(x,t)$ while keeping the reference CSA constant. That is, setting θ as constant over time (only a function of x). The relation in Eq. (3) in this case is written as

$$P = K_e \left(\frac{A(x,t)}{A_o \theta} - 1 \right) + P_o(x,t). \tag{4}$$

3.2 Peristaltic Wave Input and Active Relaxation

As mentioned above, varying the reference CSA mimics the sphincter's muscle pattern, and is obtained through the activation function θ. Different activation functions imply different muscle activity, and the function is defined based on the opening and closing modes discussed in section 2. Note that other than the activation function, the simulation set up is the same for all cases. The different activation functions are discussed next. Mathematical details on the functions themselves are available in [38, 26].

(a) Tone relaxation. This activation function simulates a contracted sphincter which relaxes and then contracts back as seen in the regular function of the AS of the US. The active relaxation of the sphincter is the only mode mechanically involved in the opening of the sphincter. Figure 3a presents this activation pattern at five consecutive time instances.

(b) Tone squeezing. This activation function simulates a scenario similar to the experimental procedure conducted by Zifan et al. [23], in which the partially relaxed sphincter contracts and then relaxes back again. This function imitates active squeezing of the FLIP bag, capturing a scenario opposite of the regular function of the AS. Figure 3b presents this activation pattern at five consecutive instances.

(c) Tone relaxation and traveling peristalsis. This activation function involves both peristaltic contraction and a tonically contracted sphincter, capturing the two mechanical modes, and is discussed in details in [26]. As the traveling peristalsis enters the domain, causing a pressure rise in the tube, the contracted sphincter starts to relax. The contraction of the tone at the end of the contractile cycle is obtained by the traveling peristalsis stopping at the sphincter location [26]. This pattern is seen in the regular function of the LES. Figure 3c presents this activation pattern at five consecutive instances.

As discussed in section 3.1, we also want to introduce a simulation where the opening and closing of the sphincter is dictated by external traction, which can be achieved by varying P_o over time. Figure 3d presents $P_o(x,t)$ at five consecutive time instances. Note that P_o in this plot is non-dimensionalized by K_e, as discussed in the next section. In these type of simulations, $\theta = \theta(x)$, as the reference CSA does not change with time. The function $\theta(x)$ takes the form of θ at the first time instance presented in Fig. 3a. In the simulations described in **(a)-(c)** above, $\theta = \theta(x,t)$ and $P_o = 0$.

3.3 Non-dimensionalizing Dynamic Equations

We use the following scales to non-dimetionalize our equations:

$$A = \alpha A_o, \qquad t = \tau t_R, \qquad u = U\frac{L}{t_R}, \qquad P = pK_e, \qquad \text{and} \qquad x = \chi L, \tag{5}$$

where α, τ, U, p, and χ are non-dimensional variables of area, time, velocity, pressure, and position, respectively [38, 39]. The terms L and t_R are dimensional constants for the the tube length and relaxation time, respectively.

Hence, the non-dimetionalized form of the mass conservation, momentum conservation, and tube law equations are

$$\frac{\partial \alpha}{\partial \tau} + \frac{\partial (\alpha U)}{\partial \chi} = \epsilon \left(\frac{\alpha}{\theta}\right)_{xx}, \tag{6}$$

$$\frac{\partial U}{\partial \tau} + U\frac{\partial U}{\partial \chi} + \psi\frac{\partial p}{\partial \chi} + \beta\frac{U}{\alpha} = 0, \qquad \text{and} \tag{7}$$

$$p = \left(\frac{\alpha}{\theta} - 1\right) + p_o - \eta\frac{\partial (\alpha U)}{\partial \chi}, \tag{8}$$

respectively. In the equations above, $\psi = K_e t_R^2/(\rho L^2)$ is the non-dimensional stiffness parameter, $\beta = 8\pi\mu t_R/(\rho A_o)$ is the non-dimensional viscosity parameter, and $p_o = P_o/K_e$ is the outside pressure. Notice that the equations above include two terms which were not included in the dimensional form of the equations. First, the term $\epsilon\left(\frac{\alpha}{\theta}\right)_{xx}$ is a smoothing term added to the right-hand side of the continuity equation in order to obtain faster convergence and reduce computational time [50]. The expression $\eta\frac{\partial(\alpha U)}{\partial \chi}$ is added to the pressure equation in order to regularize the system and therefore help stabilize the numerical solution, where $\eta = (Y A_o)/(t_R K_e)$, and Y is a damping coefficient [51]. The effect of implementing these term into the model is minimal as discussed in [38].

3.4 Boundary and Initial Conditions

The FLIP bag is closed on both ends and the volume inside it remains constant, hence,

$$U(\chi = 0, \tau) = 0 \qquad \text{and} \qquad U(\chi = 1, \tau) = 0. \tag{9}$$

Plugging this into Eq. (7), and taking the partial derivative of Eq. (8) yields a Neumann boundary condition for α, such that

$$\frac{\partial}{\partial \chi}\left(\frac{\alpha}{\theta} + p_o\right)\bigg|_{\chi=0,\tau} = 0 \qquad \text{and} \qquad \frac{\partial}{\partial \chi}\left(\frac{\alpha}{\theta} + p_o\right)\bigg|_{\chi=1,\tau} = 0. \tag{10}$$

At $\tau = 0$, the fluid inside the tube is at rest, so

$$U(\chi, \tau = 0) = 0. \tag{11}$$

Moreover, the initial CSA of the tube is defined as

$$\alpha(\chi, \tau = 0) = S_{\text{IC}}\theta(\chi, \tau = 0), \tag{12}$$

where S_{IC} is a constant area that depends on the volume of the bag. Lastly, $p_o = 0$ for all χ and τ unless specified otherwise.

3.5 Numerical Implementation

By plugging Eq. (8) into Eq. (7), we obtain a system of two equations which, together with the boundary and initial conditions in Eq. (9), Eq. (10), Eq. (11), and Eq. (12), can be used to solve for $\alpha(\chi, \tau)$ and $U(\chi, \tau)$. The MATLAB `pdepe` function is used to acquire the numerical solution, as described in greater details by [38], who also verified the code used in the 1D model by comparing it to an equivalent 3D immersed boundary simulation.

3.6 Work Decomposition

To gain a deeper understanding of the sphincters' functions, one can study the way in which energy is spent during a contraction cycle. The conservation of work equation to conduct such analysis has been derived by [38] and [26], and is briefly discussed here.

The conservation of work equation is obtained by integrating the momentum equation with respect to χ and τ, such that

$$\begin{aligned} -\psi \int_{\tau_1}^{\tau_2}\int_{\chi_1}^{\chi_2} p\frac{\partial \alpha}{\partial \tau}\mathrm{d}\chi\mathrm{d}\tau = \int_{\tau_1}^{\tau_2}\frac{\partial}{\partial \tau}\int_{\chi_1}^{\chi_2}\left(\frac{1}{2}\alpha U^2\right)\mathrm{d}\chi\mathrm{d}\tau + \beta\int_{\tau_1}^{\tau_2}\int_{\chi_1}^{\chi_2} U^2\mathrm{d}\chi\mathrm{d}\tau \\ + \psi\int_{\tau_1}^{\tau_2}(\alpha U p)\Big|_{\chi_1}^{\chi_2}\mathrm{d}\tau + \int_{\tau_1}^{\tau_2}\left(\frac{1}{2}\alpha U^3\right)\Big|_{\chi_1}^{\chi_2}\mathrm{d}\tau. \end{aligned} \tag{13}$$

The time integration boundaries, τ_1 and τ_2, are the start and end of the contraction cycle. The spacial integration boundaries, χ_1 and χ_2 mark the start and end locations of the sphincter along the tube length, where $\mathrm{w_s} = \chi_2 - \chi_1$ is the width of the sphincter. The left hand side of the equation represents the work done by the tube wall on the fluid, and the right hand side represents the consumers of this work. The consumers, in the order in which they appear in the equation, are kinetic energy of the fluid, energy loss due to viscous dissipation in the sphincter region, work done by the fluid inside the sphincter region of the fluid outside through pressure acting on the cross-section at the two ends of the sphincter, and net momentum flux.

The work done by the sphincter wall on the fluid is a result of both passive active work done by the sphincter wall on the fluid [38, 26]. The passive and active work decomposition can be applied to Eq. (13), such that

$$\begin{aligned} -\psi \int_{\tau_1}^{\tau_2}\int_{\chi_1}^{\chi_2} p_{\mathrm{active}}\frac{\partial \alpha}{\partial \tau}\mathrm{d}\chi\mathrm{d}\tau = \int_{\tau_1}^{\tau_2}\frac{\partial}{\partial \tau}\int_{\chi_1}^{\chi_2}\left(\frac{1}{2}\alpha U^2\right)\mathrm{d}\chi\mathrm{d}\tau + \beta\int_{\tau_1}^{\tau_2}\int_{\chi_1}^{\chi_2} U^2\mathrm{d}\chi\mathrm{d}\tau \\ + \psi\int_{\tau_1}^{\tau_2}(\alpha U p)\Big|_{\chi_1}^{\chi_2}\mathrm{d}\tau + \int_{\tau_1}^{\tau_2}\left(\frac{1}{2}\alpha U^3\right)\Big|_{\chi_1}^{\chi_2}\mathrm{d}\tau + \psi\int_{\tau_1}^{\tau_2}\int_{\chi_1}^{\chi_2} p_{\mathrm{passive}}\frac{\partial \alpha}{\partial \tau}\mathrm{d}\chi\mathrm{d}\tau, \end{aligned} \tag{14}$$

where the passive work is placed on the right hand side of the equation, representing the elastic energy stored in the tube wall.

Passive pressure captures the change in CSA while θ remains unchanged. The active pressure on the other hand, represents the change in the reference area as θ changes, when the CSA is fixed. The non-dimensional active and passive pressures are defined as

$$p_{\mathrm{active}}(\chi,\tau) = \alpha\left(\frac{1}{\theta(\chi,\tau)} - \frac{1}{\theta_{\mathrm{IC}}(\chi)}\right) \qquad \text{and} \qquad p_{\mathrm{passive}}(\chi,\tau) = \frac{\alpha(\chi,\tau)}{\theta_{\mathrm{IC}}(\chi)} - 1, \tag{15}$$

respectively. In the simulation where $\theta = \theta(x)$ and $p_o = p_o(\chi,\tau) \neq 0$,

$$p_{\mathrm{active}}(\chi,\tau) = 0 \qquad \text{and} \qquad p_{\mathrm{passive}}(\chi,\tau) = \frac{\alpha(\chi,\tau)}{\theta_{\mathrm{IC}}(\chi)} - 1 + p_o(\chi,\tau). \tag{16}$$

4 Results

Our simulation results discussed in this section exhibit two clear trends. A NSL (Fig. 2a) emerges when the only mechanism to open the sphincter is neurogenic mediated relaxation (mechanism (i)) or an external traction force. On the other hand, a PSL (Fig. 2b) occurs when the sphincter opens due to both neurogenic

mediated relaxation of the tone and mechanical distention (mechanisms (i) and (ii)). Hence, we reveal that the different pressure-CSA loop patterns originate from different neurally controlled muscle activities, and that the loop type is dictated by the presence or absence of the two mechanical modes proposed in section 2.

In the rest of this section, we aim to explain the above statement by looking at different simulation results, separated into two categories, based on their resulting loop type; NSL (Fig. 2a), and PSL (Fig. 2b). We investigate the different activation functions, examine what causes these loop types, and inspect how work is distributed in the system.

4.1 Negative Slope Pressure-Cross-Sectional Area Loop

As discussed in section 3.2, two different scenarios are modeled to imitate cases in which only the tone muscle constitute to the opening of the sphincters (Fig. 3a and Fig. 3b). The results exhibit that in both scenarios, a NSL emerges. The following section focuses on two simulations, each with one of these activation functions.

Figure 4 presents the results obtained by a simulation of a single contraction cycle with the activation function presented in Fig. 3a. In this simulation, the sphincter is initially contracted, then it relaxes, before contracting back to its initial tone. As the figure shows, a NSL is obtained. By tracking the five highlighted points in the figure, we can relate the total work done by the sphincter wall on the fluid to the pressure-CSA loop, which helps us to better understand the pressure-CSA relation and consequently the loop type.

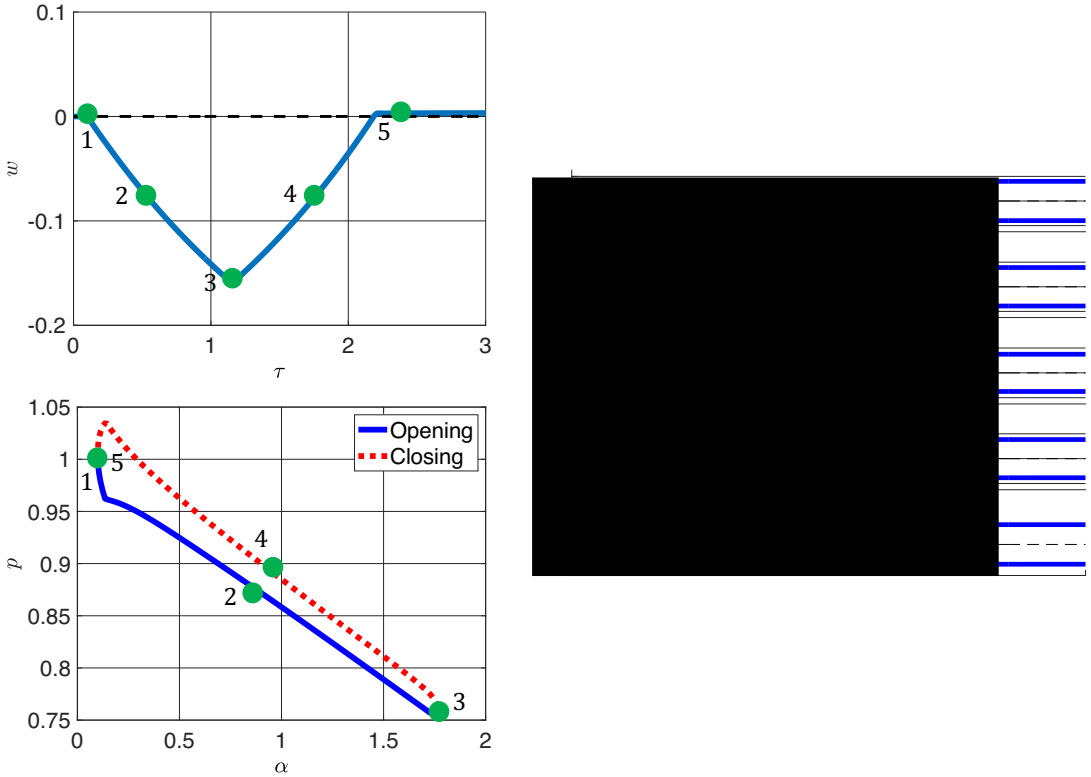

Figure 4: Simulation results of a single contraction cycle with muscle activity defined in Fig. 3a. The input parameters are set to $\beta = 100$, $\psi = 100$, and the sphincter's width is 25% of the tube length. The graph at the top left shows the curve of the cumulative total work done by the sphincter wall on the fluid normalized by ψ ($w = \text{Work}/\psi$) as a function of time. The plot at the bottom left presents the corresponding pressure-CSA loop as recorded at the sphincter location. The right plot displays the tube shape at five consecutive instants, ordered chronologically, corresponding to the five points highlighted on the two left plots.

$\boldsymbol{\tau \leq \tau_1}$. At the beginning of the contraction cycle, the sphincter is contracted. At this time instance, the wall is still and the pressure is uniform, thus, the wall does no work on the fluid. As the work curve in figure 4 shows, at this instance, the total work done by the wall on the fluid is equal to zero.

$\boldsymbol{\tau_1 < \tau < \tau_3}$. Between τ_1 and τ_3, the sphincter tone starts to actively relax, causing the CSA at the sphincter to increase. This increase is seen in the loop in Fig. 4 alongside pressure decrease. Since the sphincter opens, it does negative work on the fluid, as seen by the decrease in the total work curve in Fig. 4 between τ_1 and τ_3.

$\boldsymbol{\tau = \tau_3}$. Once $\tau = \tau_3$, the sphincter reaches its full opening, as the loop in Fig. 4 displays. Additionally, this instance corresponds to the minimum point on the work plot in the figure.

$\boldsymbol{\tau_3 < \tau < \tau_5}$. Between instances τ_3 and τ_5, the sphincter starts to contract back to its original tone, causing the CSA at the sphincter to decrease. This decrease is seen in the loop in Fig. 4 between points 3 and 5, alongside pressure increase. Since the contraction causes the sphincter to close, the sphincter squeezes the fluid, applying positive work on it. This process can be observed on the work plot in Fig. 4 which shows that between points 3 and 5, the work done by the sphincter wall on the fluid increases.

$\boldsymbol{\tau \geq \tau_5}$. Lastly, the sphincter stops contracting once it reaches its original contraction strength. The final work value is equal to the net work done by the sphincter wall of the fluid during the entire cycle.

Notice that the net total work done by the sphincter wall on the fluid is positive. This indicates that throughout this opening and closing cycle, the sphincter wall applies more work on the fluid than the fluid (through pressure) applies on the wall. As elaborated upon by [39], this loop type is called tone dominant loop (TDL), where the closing curve is above the opening curve on the pressure-CSA plot. Physically, it means that the sphincter wall needs to apply more work to contract back than the work needed to open the sphincter. This makes sense as, during closing, the wall needs to overcome fluid resistance, as elaborated upon later in this section. Note that this opening and closing pattern (closing curve above opening curve) appears in all simulations results with activation functions capturing only tone activity (Fig. 3a and Fig. 3b).

Before proceeding our discussion on how the above analysis and segmentation relates to the different loop types identified in section 2, we will consider the detailed work balance in the sphincter region. Figure 5 presents the work components in Eq. (14) and the total work term on the left hand side of Eq. (13), normalized by ψ ($w = \text{Work}/\psi$), as a function of time. As the plot shows, at $\tau = 0$, before the contracted tone starts to relax, all the work components are equal to zero. However, once relaxation begins, all curves start decreasing or increasing, each having a unique pattern. Note that the rate of change of kinetic energy and the kinetic energy flux terms (first and fourth terms on the right hand side of Eq. (14), respectively) are not plotted in the figure since $\psi >> 1$ and $\beta >> 1$ and consequently these contributions are small. In addition, recall that the spatial integration is over the sphincter region, and that each curve portrays the cumulative work done in the corresponding mode up to a given time instant.

The active work (the left hand side of Eq. (14)) is defined by the change in θ. Hence, during relaxation, θ increases and the active work done by the sphincter wall on the fluid increases, as seen in Fig. 5. As explained by [26], while the sphincter relaxes, the active pressure, as defined in Eq. (15) is negative, which implies that the fluid is sucking the sphincter's wall down. The direction of the force exerted by the wall on the fluid is same to the direction of the wall motion, so the active work is positive. The increase stops when no change in active work occurs ($\tau \approx 1.20$), which corresponds to the instance in which the tone is fully relaxed ($\theta = 1$). Once the sphincter starts to contract, θ decreases and the force exerted by the wall on the fluid is opposite to the direction of wall motion, so the active work is negative. This decrease stops when relaxation ends, where $\theta = \theta(\chi, \tau = 0)$.

Passive work (last term on the right hand side of Eq. (14)) captures the change in CSA. Since only tone relaxation controls the change in CSA in this simulation, increase, decrease and maximum relaxation occurs simultaneously to increase, decrease and maximum CSA (full opening), respectively. Hence, the passive work curve must be very close to the active work curve, both in value and trend. However, in contrast to the active work, the net passive energy stored in the sphincter wall must equal to zero since it is reversible.

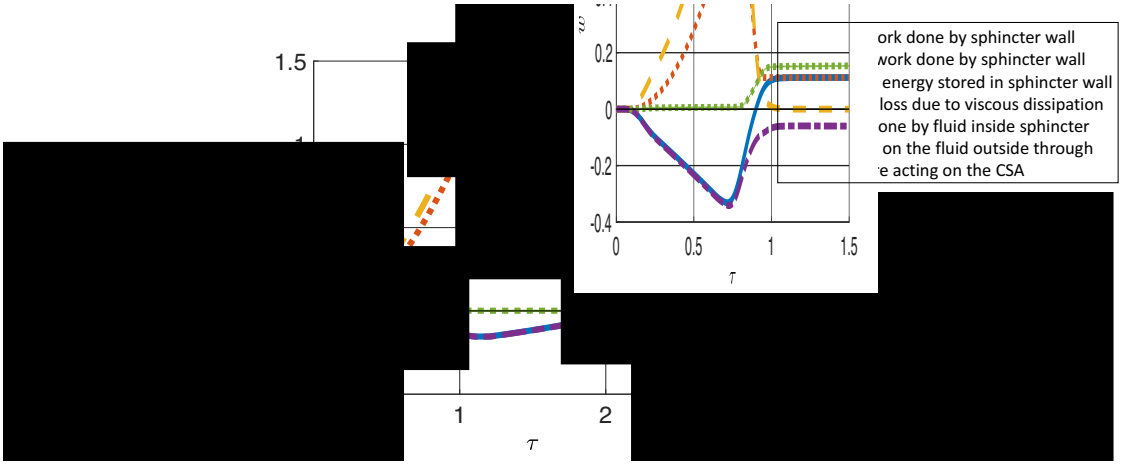

Figure 5: Plot of the work components from Eq. (14) evaluated at the sphincter region for a simulation with muscle activity defined in Fig. 3a. Each curve depicts the cumulative work done in the corresponding mode up to a given time instant. The total work done by the sphincter wall on the fluid (LHS of Eq. (13)) is also plotted. All work curves in the plot are normalized by ψ, such that $w = \text{Work}/\psi$.

The work done by the fluid inside the sphincter section on the fluid outside of the sphincter through pressure acting on the CSA at the two ends of the sphincter region (third term on the right hand side of Eq. (14)) decreases as the sphincter relaxes. This is because as the sphincter relaxes and opens, fluid from outside of the sphincter region flows into the sphincter section, which does positive work on the fluid inside. As the sphincter contracts back, an opposite affects occurs, where the contraction of the wall forces the fluid occupying the sphincter region to flow out of the sphincter region, applying positive work on the outside fluid. Notice that the value of the net work of this component is positive, meaning that fluid inside the sphincter region does more work on the fluid outside than the opposite.

The energy loss due to viscous dissipation (second term on the right hand side of Eq. (14)) maintains a steady increase throughout the contraction cycle. Since viscous dissipation cannot be recovered, the net energy that is being dissipated is positive. As the sphincter opens, viscous losses increase as a result of fluid flowing into the sphincter region. As the sphincter closes, viscous losses increase as a result of fluid flowing out of the sphincter region.

Understanding the trends of the viscous losses and the work done on the fluid within the sphincter region by the pressure imposed on the cross-sections at the two ends of the sphincter region (negative of the third term on the right hand side of Eq. (14)) is particularly useful. They explain why the net total work done by the sphincter wall on the fluid is positive. During opening, fluid outside of the sphincter region flows into the sphincter region by pressure gradient. On the other hand, during closing, the wall itself applies the work to push the fluid occupying the relaxed sphincter segment away through the two ends of the sphincter region, while overcoming fluid resistance.

The above discussion and the time decomposition into the five stages presented in Fig. 4 explain the shape of the loop. In this simulation, tone activity is the only component that controls the change of CSA of the sphincter, with relaxation and contraction corresponding to opening and closing of the sphincter, respectively. Pressure change is directly related to the change in the shape of the elastic tube. Thus, with no additional pressurization source in the form of contraction elsewhere along the tube length, tone activity is the only stimulus that results in pressure change in the tube. By elementary physics, if no other pressurization source is applied as the sphincter relaxes and the CSA increases, then pressure must drop. As the sphincter contracts, CSA decreases while pressure increases back up.

As long as tone relaxation is the only component resulting in the opening of the sphincter, a NSL emerges, independent of the order of operations. For instance, Fig. 6 presents the results of a simulation with activation function defined in Fig. 3b, where a relaxed sphincter contracts and then relaxes back. As

the figure shows, this simulation also resulted in a NSL (bottom right plot).

The left plot, presenting the work components in Eq. (14), provides an insight into the underlying mechanism relating pressure and CSA in this case. As the figure shows, the total work done by the sphincter on the fluid (left hand side of Eq. (13)) has the opposite trend to the curve in Fig. 4. This is because in this simulation, the sphincter wall first contracts, doing positive work on the fluid (total work curve increases) and then relaxes, doing negative work on the fluid (total work curve decreases). This trend, although opposite, captures the same mechanism which results in a NSL. Initially, the bag in the tube is pressurized while the sphincter is mostly open. Hence, once the sphincter starts to contract, decreasing CSA, the pressure in the bag increases, resulting in a negative slope curve between pressure and CSA. This is the pattern that is observed in AS experimental set up by [23]. Similar to the results in Fig. 4, the net total work done by the wall on the fluid in Fig. 6 is positive, indicating that the wall does more work on the fluid than the fluid (through pressure) does on the wall throughout this opening and closing cycle.

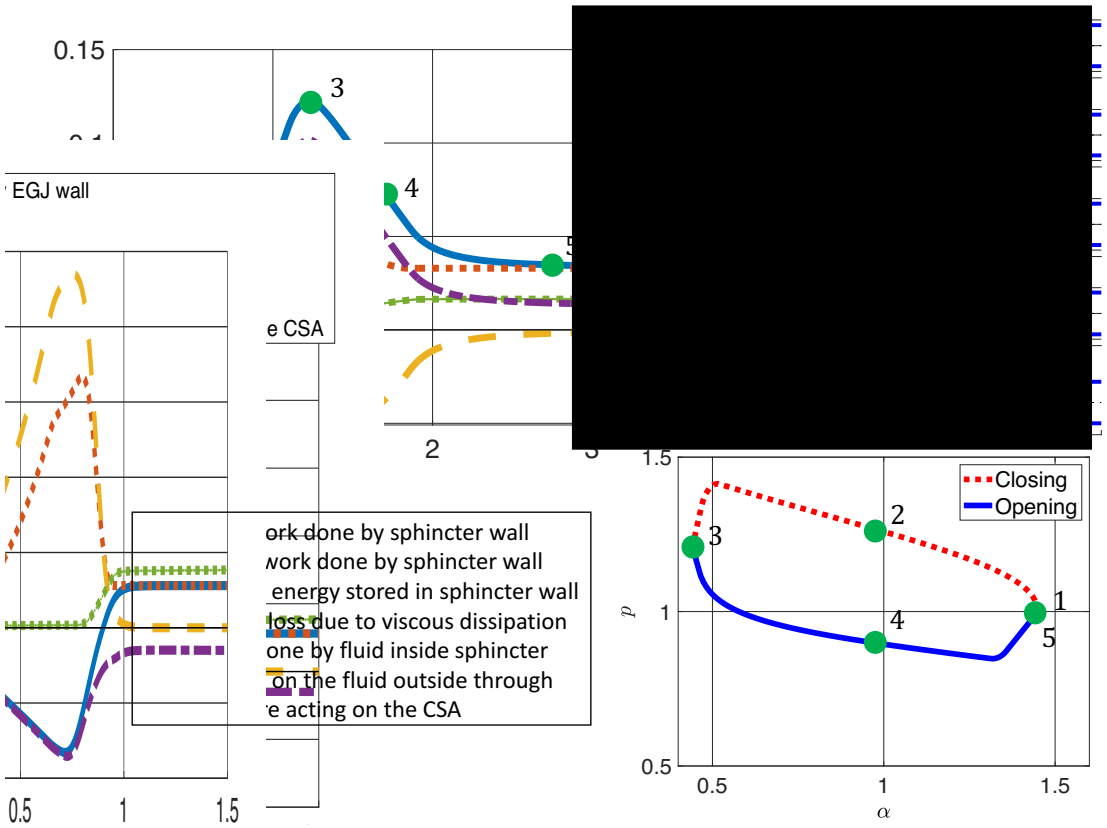

Figure 6: Simulation results of a single contraction cycle with muscle activity defined in Fig. 3b. The input parameters are set to $\beta = 5000$, $\psi = 100$, and the sphincter's width is 25% of the tube length. The left plot shows the curves of the cumulative work components from Eq. (14) evaluated at the sphincter region and the curve of the cumulative total work done by the sphincter wall on the fluid (LHS of Eq. (13)) as a function of time. The work terms are normalized by ψ. The plot at the bottom right presents the corresponding pressure-CSA loop as recorded at the sphincter location. The top right plot displays the tube shape at five consecutive instants, ordered chronologically, corresponding to the five points highlighted on the two left plots. The larger β value compared to the other simulations is chosen to show the effect of fluid viscosity on the result.

It is also interesting to look at the passive and active decomposition of the total work, as the trends are slightly different than the ones discussed in Fig. 5. In the simulation discussed in Fig. 6, the active work

done by the sphincter wall on the fluid has a similar trend to the one previously described. The active work done by the sphincter wall on the fluid increases as the wall contracts, because the direction of the force exerted by the wall on the fluid is pointed in the same direction as the wall motion. When the sphincter reaches maximum contraction, it reaches its minimum CSA and there is no change in active work. Once the sphincter starts to relax back, CSA increases, and the active work done by the sphincter wall on the fluid begins to decrease since the force exerted by the wall on the fluid is opposite to the direction of wall motion. The elastic energy stored in the tube wall in this simulation has an opposite pattern than the one described before (Fig. 5). Since the CSA decreases as a direct result of squeezing, passive work, which captures this change, is negative.

Notice that the area between the opening and closing curves in Fig. 6 is much greater than the one in Fig. 4. As elaborated upon in [26], the loop area indicates that there is some energy that is being gained or lost by the system. If the closing curve is above the opening curve, as in the two cases discussed above, energy is being lost, meaning that the sphincter does most of the work in the opening and closing cycle (as opposed to pressure from the fluid). Thus, the larger the area between the two curves, the more energy the sphincter tone needs to expend. The sphincter wall applies more work in the example presented in Fig. 6 than the one in Fig. 4. This difference is mostly due to the value of β (equivalent to increasing fluid viscosity). Increasing fluid viscosity (by increasing β) implies increasing flow resistance in this case [39], which requires more work from the wall in order to contract. The effect of viscosity is further discussed in [26].

Note that a NSL is also observed from simulations where θ does not vary in time but $p_o = p_o(\chi, \tau)$, as in the UES. In these simulations, Eq. (4) is used for the constitutive pressure relation, where $p_o(\chi, \tau)$ is illustrated in Fig. 3d. Figure 7 presents the results obtained by a simulation of this set up. These results emphasize once again that when the sphincter opens due to mechanism (i), a NSL emerges. Furthermore, it strengthens the argument that the mechanical imprint of the pressure-CSA loop does not change whether the opening is due to neurogenic mediated relaxation or neurally controlled external pulling. The mechanical picture of both scenarios is equivalent and therefore labeled as mechanism (i). Notice that the change in CSA is smaller than the one obtained from simulations where the sphincter opens by muscle relaxation (change reference CSA). This is simply because changing external pressure in the simulation context is not as effective as varying reference CSA.

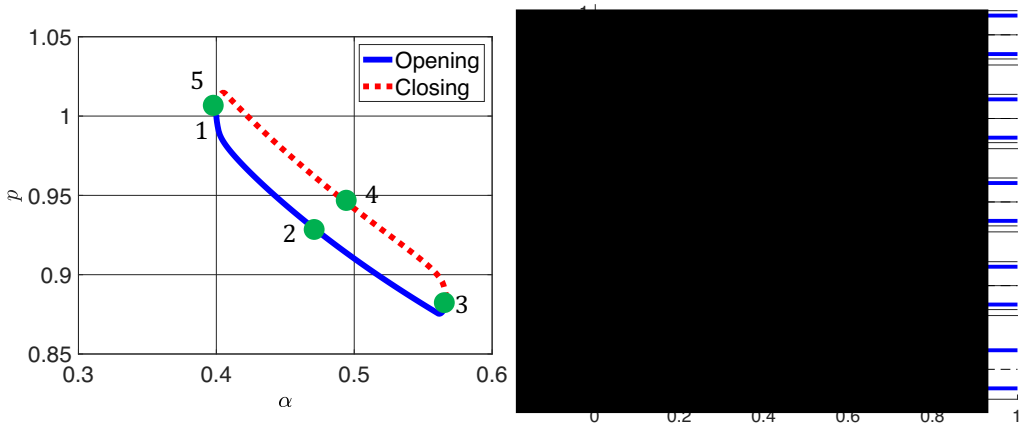

Figure 7: Simulation results of a single contraction cycle with constant reference CSA but varying external pressure, p_o (Fig. 3d). The input parameters are set to $\beta = 100$, $\psi = 100$, and the sphincter's width is 25% of the tube length. Pressure-CSA loop at the sphincter location (left) and the tube shapes at five consecutive instants (right).

4.2 Positive Slope Pressure-Area Loop

Figure 8 presents the results obtained by a simulation of a single contraction cycle with the activation function presented in Fig. 3c, where the muscle activity is defined by both a sphincter tone and a traveling peristalsis. As the figure shows, a PSL emerges. Hence, the results suggest that when the sphincter opening pattern involves both mechanical distention and neurogenic mediated opening, as in the case of the LES, a PSL is obtained. The reason for that lies in the way in which the activation function dictates the pressure in the tube. In the previous two cases (Fig. 4 and Fig.6), when the sphincter tone starts to relax, the sphincter's CSA increases, and consequently the pressure decreases. In this case (Fig. 8), a similar process takes place, however, as sphincter relaxation starts, a peristaltic contraction begins traveling down the tube length, which increases pressure that mechanically helps in opening the sphincter.

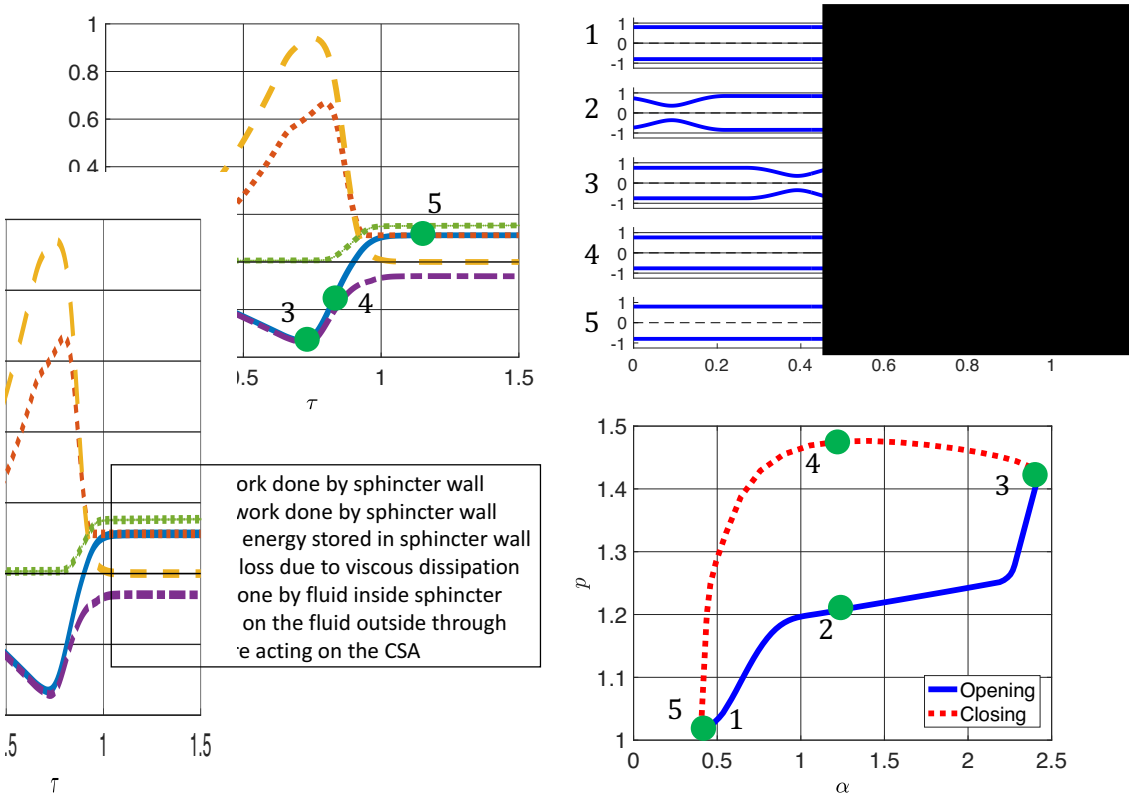

Figure 8: Simulation results of a single contraction cycle with muscle activity defined by a neurally controlled tone relaxation and a traveling peristalsis (Fig. 3c). The input parameters are set to $\beta = 100$ and $\psi = 100$. The widths of the traveling wave and the sphincter are each set to 25% of the tube length. The left plot shows the curves of the cumulative work components from Eq. (14) evaluated at the sphincter region and the curve of the cumulative total work done by the sphincter wall on the fluid (LHS of Eq. (13)) as a function of time. The work terms are normalized by ψ. The plot at the bottom right presents the corresponding pressure-CSA loop as recorded at the sphincter location. The top right plot displays the tube shape at five consecutive instants, ordered chronologically corresponding to the highlighted points on the loop and work plots.

As figure 8 shows, the individual work curves follow similar patterns to the ones appear in figure 5. This is simply because the CSA of the sphincter changes in the same way (i.e., contracted → relaxed → contracted). The main difference between the two plots is in the passive work curve, which is a lot larger than the active work curve in Fig. 8 as opposed to Fig. 5. This trend results in the two pressure-CSA patterns. The passive

work in Fig. 8 is much larger than the active work because it increases as a result of mechanical distention created by the peristaltic contraction wave in addition to tone relaxation.

5 Discussion

Knowing what is the controlling mechanism that dictates the pressure-CSA loop types at the different sphincters has several useful applications. First, we can use this to hypothesize how the pressure-CSA loops will look for sphincters where data is not available. For instance, limited work has been done to study the US using a fluid filled bag at constant volume and we did not find any such studies capturing the opening and closing trends of the US during a contraction cycle. Knowing that the US opening and closing cycle is controlled by tone relaxation, we can hypothesize that US pressure-CSA plots throughout single cycles will display a negative slope. The loop type for each sphincter, based on the information revealed in this study, is hypothesized and listed in table 4. Second, we can use information from the pressure-CSA loops to identify normal and abnormal phenotypes for the different sphincters. Lastly, calculating the work done by the sphincter can help in creating a physiomarker. This can be used as a diagnostic tool to evaluate pathophysiologies of sphincters.

Table 4: Human sphincters and the hypothesized resulting pressure-CSA loops obtained by FLIP experiments

Sphincter	**Description**
Upper esophageal sphincter	Negative slope
Lower esophageal sphincter	Positive slope
Pyloric sphincter	Positive slope
Sphincter of Oddi	Negative slope
Internal anal sphincter	Negative slope
External anal sphincter	Negative slope
Urethral sphincter	Negative slope

Although both peristalsis and tone relaxation are present at the SoO, clinical data reveals that the SoO pressure-CSA relation depicts negative slope characteristics [27]. Recall that the loop type depends on the amount of pressurization and the timing of the opening/relaxation of the sphincter itself. Thus, this indicates that relaxation dominates the opening of the SoO and the pressurization has little effect.

Since the PS opening and closing cycle during the inter-digestive state is controlled by peristalsis and tone relaxation, we hypothesized in table 4 that PS pressure-CSA plots throughout single cycles will display a positive slope. However, depending on the amount of pressurization, the PS could behave as the LES or could have a different response like the SoO. This hypothesis can be validated or dismissed through further clinical investigation.

Note that the loop types and their underlying mechanisms discussed in this report only hold for FLIP manometry measurements of a constant volume fluid filled bag. Other measuring devices which relate pressure and CSA may result in different loop patterns. For example, high-resolution manometry has been used by many to measure pressure and CSA at different sphincters [52, 53, 54, 55, 56, 57, 58, 59, 60, 61]. Similar to the FLIP, it can be used to relate changes in CSA and the corresponding changes in pressure, recorded at the same instance and location [62, 55, 63]. However, few studies have plotted the pressure-CSA hysteresis and attempted to explain the observations. [53] and [52] plotted the pressure-CSA relation at the UES using high-resolution manometry and classified possible mechanical states of the UES muscle, which take place during the opening and closing cycle. Their results reveal an L-shaped pressure-CSA relation. These observations are not reproduced nor discussed in this work, but should be the subject for further investigation.

Declarations

Ethical approval

N/A

Acknowledgments

This work was funded by the by the National Institutes of Health (NIDDK grants DK079902 & DK117824 and NIDDK grants DK079902), and National Science Foundation (OAC grants 1450374 & 1931372)

Conflict of interest

Peter J. Kahrilas, and John E. Pandolfino hold shared intellectual property rights and ownership surrounding FLIP panometry systems, methods, and apparatus with Medtronic Inc.

Dustin A. Carlson: Medtronic (Speaking, Consulting)

Wenjun Kou: Crospon, Inc. (Consulting)

Peter J. Kahrilas: Ironwood (Consulting), Reckitt (Consulting), Johnson & Johnson (Consulting)

John E. Pandolfino: Crospon, Inc (stock options), Given Imaging (Consultant, Grant, Speaking), Sandhill Scientific (Consulting, Speaking), Takeda (Speaking), Astra Zeneca (Speaking), Medtronic (Speaking, Consulting), Torax (Speaking, Consulting), Ironwood (Consulting), Impleo (Grant)

Author contributions

Guy Elisha wrote the main manuscript text and prepared all the figures; Guy Elisha and Sourav Halder wrote the code; Neelesh A. Patankar and Guy Elisha developed the mathematical formulation; Dustin A. Carlson and Wenjun Kou contributed to data acquisition; Guy Elisha, Sourav Halder, Dustin A. Carlson, Wenjun Kou, Peter J. Kahrilas, John E. Pandolfino, and Neelesh A. Patankar interpreted results of calculations; Peter J. Kahrilas, John E. Pandolfino, and Neelesh A. Patankar contributed to obtaining funding, critical revision of the manuscript and final approval.

References

[1] Hershcovici, T., Mashimo, H., and Fass, R., 2011. "The lower esophageal sphincter". *Neurogastroenterology and motility,* **23**(9), June, pp. 819–830.

[2] Gregersen, H., and Lo, K. M., 2018. "What is the future of impedance planimetry in gastroenterology?". *Neurogastroenterology and motility,* **24**(2), Apr., pp. 166–181.

[3] Pandolfino, J. E., Shi, G., Trueworthy, B., and Kahrilas, P. J., 2003. "Esophagogastric junction opening during relaxation distinguishes nonhernia reflux patients, hernia patients, and normal subjects". *Gastroenterology,* **125**(4), Oct., pp. 1018–1024.

[4] Kahrilas, P. J., 2008. "Gastroesophageal reflux disease". *The New England journal of medicine,* **359**(16), Oct., pp. 1700–1707.

[5] Boeckxstaens, G. E., Zaninotto, G., and Richter, J. E., 2014. "Achalasia". *The Lancet,* **393**(9911), Jan., pp. 83–93.

[6] Eckardt, A. J., and Eckardt, V. F., 2009. "Current clinical approach to achalasia". *World journal of gastroenterology,* **15**(32), Aug., p. 3969–3975.

[7] Kahrilas, P. J., 2022. "Retrograde upper esophageal sphincter function... and dysfunction". *Neurogastroenterology & Motility,* **34**(5), p. e14328.

[8] Sivarao, D., and Goyal, R. K., 2000. "Functional anatomy and physiology of the upper esophageal sphincter". *The American journal of medicine,* **108**(4), Mar., pp. 27–37.

[9] Patel, R. V., and Hirano, I., 2018. "Endoscopic diagnosis and treatment of disorders of upper esophageal sphincter function". *Techniques in Gastrointestinal Endoscopy,* **20**(3), pp. 139–145.

[10] Preiksaitis, H. G., Tremblay, L., and Diamant, N. E., 1994. "Nitric oxide mediates inhibitory nerve effects in human esophagus and lower esophageal sphincter". *Digestive diseases and sciences,* **39**(4), pp. 770–775.

[11] Mittal, R. K., and Balaban, D. H., 1997. "The esophagogastric junction". *The New England Journal of Medicine,* **336**(13), Mar., pp. 924–932.

[12] Moore, K. L., and Dalley, A. F., 2018. *Clinically oriented anatomy.* Wolters kluwer india Pvt Ltd.

[13] Shafik, A., El Sibai, O., Shafik, A. A., et al., 2006. "Mechanism of gastric emptying through the pyloric sphincter: a human study". *Medical Science Monitor,* **13**(1), pp. CR24–CR29.

[14] Woods, C. M., Mawe, G., Toouli, J., and Saccone, G., 2005. "The sphincter of oddi: understanding its control and function". *Neurogastroenterology & Motility,* **17**, pp. 31–40.

[15] Meunier, P., and Mollard, P., 1977. "Control of the internal anal sphincter (manometric study with human subjects)". *Pflügers Archiv,* **370**(3), pp. 233–239.

[16] Jung, J., Ahn, H. K., and Huh, Y., 2012. "Clinical and functional anatomy of the urethral sphincter". *International neurourology journal,* **16**(3), p. 102.

[17] De Groat, W., and Theobald, R., 1976. "Reflex activation of sympathetic pathways to vesical smooth muscle and parasympathetic ganglia by electrical stimulation of vesical afferents". *The Journal of Physiology,* **259**(1), pp. 223–237.

[18] Chancellor, M. B., and Yoshimura, N., 2004. "Neurophysiology of stress urinary incontinence". *Reviews in urology,* **6**(Suppl 3), p. S19.

[19] Sam, P., Jiang, J., and LaGrange, C. A., 2020. "Anatomy, abdomen and pelvis, sphincter urethrae". *StatPearls [Internet].*

[20] Yucel, S., and Baskin, L. S., 2004. "An anatomical description of the male and female urethral sphincter complex". *The Journal of urology,* **171**(5), pp. 1890–1897.

[21] Hirano, I., Pandolfino, J. E., and Boeckxstaens, G. E., 2017. "Functional lumen imaging probe for the management of esophageal disorders: Expert review from the clinical practice updates committee of the aga institute". *Clinical gastroenterology and hepatology,* **15**(3), Mar., pp. 325–334.

[22] Lottrup, C., Gregersen, H., Liao, D., Fynne, L., Frøkjær, J. B., Krogh, K., Regan, J., Kunwald, P., and McMahon, B. P., 2015. "Functional lumen imaging of the gastrointestinal tract". *Journal of gastroenterology,* **50**(10), May, pp. 1005–1016.

[23] Zifan, A., Mittal, R. K., Kunkel, D. C., Swartz, J., Barr, G., , and Tuttle, L. J., 2019. "Loop analysis of the anal sphincter complex in fecal incontinent patients using functional luminal imaging probe". *American journal of physiology: Gastrointestinal and liver physiology,* **318**(1), Nov., pp. G66–G76.

[24] Carlson, D. A., Lin, Z., Kahrilas, P. J., Sternbach, J., Donnan, E. N., Friesen, L., Listernick, Z., Mogni, B., and Pandolfino, J. E., 2015. "The functional lumen imaging probe detects esophageal contractility not observed with manometry in patients with achalasia". *Gastroenterology,* **149**(7), Dec., pp. 1742–1751.

[25] Gregersen, H., and Christensen, J., 2016. *Clinical mechanics in the gut: an introduction.* Bentham Science Publishers.

[26] Elisha, G., Halder, S., Acharya, S., Carlson, D. A., Kou, W., Kahrilas, P. J., Pandolfino, J. E., and Patankar, N. A., 2023. "A mechanics-based perspective on the function of the esophagogastric junction during functional luminal imaging probe manometry". *Biomechanics and Modeling in Mechanobiology*, pp. 1–19.

[27] Kunwald, P., Drewes, A. M., Kjaer, D., Gravesen, F. H., McMahon, B., Madácsy, L., Funch-jensen, P., and Gregersen, H., 2010. "A new distensibility technique to measure sphincter of oddi function". *Neurogastroenterology & Motility,* **22**(9), pp. 978–e253.

[28] Klarskov, N., and Lose, G., 2007. "Urethral pressure reflectometry; a novel technique for simultaneous recording of pressure and cross-sectional area in the female urethra". *Neurourology and Urodynamics: Official Journal of the International Continence Society,* **26**(2), pp. 254–261.

[29] Aagaard, M., Klarskov, N., Sønksen, J., Bagi, P., Colstrup, H., and Lose, G., 2012. "Urethral pressure reflectometry; a novel technique for simultaneous recording of pressure and cross-sectional area: a study of feasibility in the prostatic urethra". *BJU international,* **110**(8), pp. 1178–1183.

[30] Khayyami, Y., Klarskov, N., and Lose, G., 2016. "The promise of urethral pressure reflectometry: an update". *International urogynecology journal,* **27**(10), pp. 1449–1458.

[31] Regan, J., Walshe, M., Rommel, N., and McMahon, B., 2013. "A new evaluation of the upper esophageal sphincter using the functional lumen imaging probe: a preliminary report". *Diseases of the Esophagus,* **26**(2), pp. 117–123.

[32] Kwiatek, M. A., Pandolfino, J. E., Hirano, I., and Kahrilas, P. J., 2010. "Esophagogastric junction distensibility assessed with an endoscopic functional luminal imaging probe (endoflip)". *Gastrointestinal endoscopy,* **72**(2), Aug., pp. 272–278.

[33] Gourcerol, G., Tissier, F., Melchior, C., Touchais, J., Huet, E., Prevost, G., Leroi, A., and Ducrotte, P., 2015. "Impaired fasting pyloric compliance in gastroparesis and the therapeutic response to pyloric dilatation". *Alimentary Pharmacology & Therapeutics,* **41**(4), pp. 360–367.

[34] Malik, Z., Sankineni, A., and Parkman, H., 2015. "Assessing pyloric sphincter pathophysiology using endo flip in patients with gastroparesis". *Neurogastroenterology & Motility,* **27**(4), pp. 524–531.

[35] Gourcerol, G., Granier, S., Bridoux, V., Menard, J., Ducrotté, P., and Leroi, A., 2016. "Do endoflip assessments of anal sphincter distensibility provide more information on patients with fecal incontinence than high-resolution anal manometry?". *Neurogastroenterology & Motility,* **28**(3), pp. 399–409.

[36] Schuster, M. M., Hendrix, T. R., Mendeloff, A. I., et al., 1963. "The internal anal sphincter response: manometric studies on its normal physiology, neural pathways, and alteration in bowel disorders". *The Journal of clinical investigation,* **42**(2), pp. 196–207.

[37] Burleigh, D. E., and D'Mello, A., 1983. "Neural and pharmacologic factors affecting motility of the internal anal sphincter". *Gastroenterology,* **84**(2), pp. 409–417.

[38] Acharya, S., Kou, W., Halder, S., Carlson, D. A., Kahrilas, P. J., Pandolfino, J. E., and Patankar, N. A., 2021. "Pumping patterns and work done during peristalsis in finite-length elastic tubes". *Journal of Biomechanical Engineering,* **143**(7), Mar.

[39] Elisha, G., Acharya, S., Halder, S., Carlson, D. A., Kou, W., Kahrilas, P. J., Pandolfino, J. E., and Patankar, N. A., 2023. "Peristaltic regimes in esophageal transport". *Biomechanics and Modeling in Mechanobiology,* **22**(1), pp. 23–41.

[40] Hirano, I., 2015. "Esophagus: Anatomy and structural anomalies". *Yamada's Textbook of Gastroenterology*, pp. 42–59.

[41] Hellström, P. M., Grybäck, P., and Jacobsson, H., 2006. "The physiology of gastric emptying". *Best Practice & Research Clinical Anaesthesiology,* **20**(3), pp. 397–407.

[42] Deloose, E., Janssen, P., Depoortere, I., and Tack, J., 2012. "The migrating motor complex: control mechanisms and its role in health and disease". *Nature reviews Gastroenterology & hepatology,* **9**(5), pp. 271–285.

[43] Hunt, J., 1983. "Mechanisms and disorders of gastric emptying". *Annual review of medicine,* **34**(1), pp. 219–229.

[44] Kuussayer, T., Ducker, T. E., Clench, M. H., and Mathias, J. R., 1995. "Ampulla of vater/duodenal wall spasm diagnosed by antroduodenal manometry". *Digestive diseases and sciences,* **40**(8), pp. 1710–1719.

[45] Ottesen, J., 2003. "Valveless pumping in a fluid-filled closed elastic tube-system: one-dimensional theory with experimental validation". *Journal of Mathematical Biology,* **46**(4), Apr., pp. 309–332.

[46] Whittaker, R. J., Heil, M., Jensen, O. E., and Waters, S. L., 2010. "A rational derivation of a tube law from shell theory". *The Quarterly Journal of Mechanics and Applied Mathematics,* **63**(4), Aug., pp. 465–496.

[47] Kwiatek, M. A., Hirano, I., Kahrilas, P. J., Rothe, J., Luger, D., and Pandolfino, J. E., 2011. "Mechanical properties of the esophagus in eosinophilic esophagitis". *Gastroenterology,* **140**(1), Jan., pp. 82–90.

[48] Bringley, T. T., Childress, S., Vandenberghe, N., and Zhang, J., 2008. "An experimental investigation and a simple model of a valveless pump". *Physics of Fluids,* **20**(3), Mar., p. 033602.

[49] Manopoulos, C. G., Mathioulakis, D. S., and Tsangaris, S. G., 2006. "One-dimensional model of valveless pumping in a closed loop and a numerical solution". *Physics of Fluids,* **18**(1), Jan., p. 017106.

[50] LeVeque, R. J., 1990. *Numerical Methods for Conservation Laws.* Birkhäuser Basel.

[51] Wang, X., Fullana, J.-M., and Lagrée, P.-Y., 2014. "Verification and comparison of four numerical schemes for a 1d viscoelastic blood flow model". *Computer Methods in Biomechanics and Biomedical Engineering,* **18**(15), Aug., pp. 1704–1725.

[52] Omari, T. I., Jones, C. A., Hammer, M. J., Cock, C., Dinning, P., Wiklendt, L., Costa, M., and McCulloch, T. M., 2016. "Predicting the activation states of the muscles governing upper esophageal sphincter relaxation and opening". *American Journal of Physiology-Gastrointestinal and Liver Physiology,* **310**(6), pp. G359–G366.

[53] Omari, T. I., Wiklendt, L., Dinning, P., Costa, M., Rommel, N., and Cock, C., 2015. "Upper esophageal sphincter mechanical states analysis: a novel methodology to describe ues relaxation and opening". *Frontiers in Systems Neuroscience,* **8**, Jan., p. 241.

[54] Lin, Z., Yim, B., Gawron, A., Imam, H., Kahrilas, P. J., and Pandolfino, J. E., 2014. "The four phases of esophageal bolus transit defined by high-resolution impedance manometry and fluoroscopy". *American Journal of Physiology-Gastrointestinal and Liver Physiology,* **307**(4), pp. G437–G444.

[55] Carlson, D. A., and Pandolfino, J. E., 2015. "High-resolution manometry in clinical practice". *Gastroenterology & hepatology,* **11**(6), p. 374.

[56] Kirby, A. C., Tan-Kim, J., and Nager, C. W., 2015. "Measurement of dynamic urethral pressures with a high resolution manometry system in continent and incontinent women". *Female pelvic medicine & reconstructive surgery,* **21**(2), p. 106.

[57] Desipio, J., Friedenberg, F., Korimilli, A., Richter, J., Parkman, H., and Fisher, R., 2007. "High-resolution solid-state manometry of the antropyloroduodenal region". *Neurogastroenterology & Motility,* **19**(3), pp. 188–195.

[58] Wasenda, E. J., Kirby, A. C., Lukacz, E. S., and Nager, C. W., 2018. "The female continence mechanism measured by high resolution manometry: Urethral bulking versus midurethral sling". *Neurourology and urodynamics,* **37**(5), pp. 1809–1814.

[59] Vitton, V., Ben Hadj Amor, W., Baumstarck, K., Behr, M., Bouvier, M., and Grimaud, J.-C., 2013. "Comparison of three-dimensional high-resolution manometry and endoanal ultrasound in the diagnosis of anal sphincter defects". *Colorectal Disease,* **15**(10), pp. e607–e611.

[60] Carrington, E. V., Brokjaer, A., Craven, H., Zarate, N., Horrocks, E., Palit, S., Jackson, W., Duthie, G., Knowles, C., Lunniss, P., et al., 2014. "Traditional measures of normal anal sphincter function using high-resolution anorectal manometry (hram) in 115 healthy volunteers". *Neurogastroenterology & Motility,* **26**(5), pp. 625–635.

[61] Jones, M. P., Post, J., and Crowell, M. D., 2007. "High-resolution manometry in the evaluation of anorectal disorders: a simultaneous comparison with water-perfused manometry". *Official journal of the American College of Gastroenterology— ACG,* **102**(4), pp. 850–855.

[62] Kahrilas, P. J., Bredenoord, A. J., Fox, M., Gyawali, C. P., Roman, S., Smout, A. J., Pandolfino, J. E., and Group, I. H. R. M. W., 2015. "The chicago classification of esophageal motility disorders, v3. 0". *Neurogastroenterology & Motility,* **27**(2), pp. 160–174.

[63] Pandolfino, J. E., Zhang, Q. G., Ghosh, S. K., Han, A., Boniquit, C., and Kahrilas, P. J., 2006. "Transient lower esophageal sphincter relaxations and reflux: mechanistic analysis using concurrent fluoroscopy and high-resolution manometry". *Gastroenterology,* **131**(6), pp. 1725–1733.